frontiers | Frontiers in Physics

TYPE Original Research
PUBLISHED 09 May 2023
DOI 10.3389/fphy.2023.1192965

OPEN ACCESS

EDITED BY
Zhenxu Bai,
Hebei University of Technology, China

REVIEWED BY
Jian Li,
Taiyuan University of Technology, China
Xu Wu,
Shenzhen Technology University, China

*CORRESPONDENCE
Guochen Wang,
wanggc@hit.edu.cn

RECEIVED 24 March 2023
ACCEPTED 20 April 2023
PUBLISHED 09 May 2023

CITATION
Gao H, Wang G, Gao W, Zhao B, Zhang R, Zhang B and Yang F (2023), An impact-insensitive fiber optic current transformer based on polarization maintaining photonic crystal fiber delay coil. *Front. Phys.* 11:1192965. doi: 10.3389/fphy.2023.1192965

An impact-insensitive fiber optic current transformer based on polarization maintaining photonic crystal fiber delay coil

Hongze Gao[1], Guochen Wang[1]*, Wei Gao[1], Bo Zhao[1,2], Runfeng Zhang[2], Boya Zhang[3] and Fan Yang[4]

[1]School of Instrumentation Science and Engineering, Harbin Institute of Technology, Harbin, China, [2]HIT (An Shan) Institute of Industrial Technology, Anshan, China, [3]Military Office of Rocket Armaments Department in Harbin District, Harbin, China, [4]Shaanxi Dongfang Aviation Instrument Co., Ltd., Hanzhong, China

When the polarization-maintaining fiber (PMF) delay coil of a fiber optic current transformer (FOCT) is impacted, external forces on the optical fibers and change of their birefringence may lead to extra phase errors during the propagation of optical signals in the fibers. These errors increase the error in current measurement. In the paper, the environmental impact mechanisms influencing the PMF delay coil of FOCT were investigated with a mathematical error model. The method of replacing PMF with a polarization-maintaining photonic crystal fiber (PCF) as the delay coil was proposed. Also, the relationship between structural parameters of air holes and linear birefringence of the polarization maintaining PCF subjected to stress was investigated. The structural parameters of optical fibers were also optimized subsequently. Simulated impact experiments of FOCT with polarization-maintaining PCF and PMF as the delay coil, respectively, demonstrated the effective impact resistance of FOCT with polarization-maintaining PCF delay coil after the optimization of its structural parameters. The current measurement errors of the FOCTs with polarization maintaining PCF delay coil reduced by approximately 35% with respect to the FOCT with PMF delay coil.

KEYWORDS

polarization maintaining fiber delay coil, fiber optic current transformer, polarization maintaining photonic crystal fiber, environmental impact, current measurement error

1 Introduction

As a kind of current transformer based on the Faraday effect, the fiber optic current transformer (FOCT) can be used as one of the key test instruments for the ship's integrated power system due to its good insulation and high reliability or later [1–6]. Due to the high-energy weapons (electromagnetic guns, laser systems, *etc.*) and detection systems equipped in modern ships, the impact and large ambient temperature fluctuations resulting from the impulse load greatly increase the current measurement error of FOCT. This error increase causes the protection circuit on the ship to trigger incorrectly [7–9]. Consequently, the FOCT loses its original monitoring and control function of the integrated power system of the ship. Therefore, the integrated power system of the ship puts forward higher requirements on the environmental adaptability of the FOCT.

As one of the important applications of FOCT, the integrated power system of a ship has been proposing the requirements of high environmental adaptability to FOCT, which mainly involves adaptability to temperature and impact. Reference [10] proposed the appropriate delay length of a $\lambda/4$ wave plate to compensate for the change in the Verdet constant of a fiber sensing coil, which could compensate for the influence of temperature on current measurement error well. So we need to focus on the effect of environmental impact on the FOCT and compensate for the current measurement error.

The effect of external impacts on FOCT is mainly through a polarization-maintaining fiber (PMF) delay coil [11], but the winding method of the PMF delay coil has not been taken into consideration so far in the research. In fact, different layers of a fiber coil have different forces. Reference [12] analyzed the forces of a PMF delay coil under an impact environment and established a resulting phase error model. However, the model is not applicable to FOCT, and the error model needs to be rebuilt to analyze the relationship between environmental impact and current measurement error quantitatively. In addition, there have been no studies to provide a suitable solution for the current measurement error of FOCT caused by an impact. Taking practical application into account, the requirements for FOCT to be lightweight and of small size are proposed, so adding an impact-proof shell to FOCT cannot satisfy our requirements. Therefore, we believe that it is of great significance to establish the error model of impacts on a fiber delay coil and to explore appropriate solutions.

In the article, we first analyzed the force of the PMF delay coil in in-line Sagnac FOCT under an impact condition. We subsequently established the phase error model of the fiber delay coil and revealed the essential relationship between linear birefringence, phase error, and current measurement error. Based on this error model, a polarization-maintaining photonic crystal fiber (PCF) was proposed to replace PMF as the delay coil. Then, the change of linear birefringence under forces of polarization maintaining PCFs with different sectional structural parameters was analyzed. Based on the analysis, the structural parameters of the polarization maintaining PCF were optimized. The study proved that the linear birefringence fluctuation of the PCF with the optimized structural parameters is smaller compared to that of the PMF under the impact environment in theory. Finally, this study verified the accuracy and rationality of the model and confirmed the effectiveness of the proposed solution using the two types of optical fibers. The optical fibers were used for the test of the current measurement error of the FOCT fiber delay coil under the normal and the impact environments, respectively. It is proved that the proposed solution can improve the current measurement stability of the FOCT under impact by using the optimized design of the polarization-maintaining PCF delay coil.

2 The establishment of the error model of FOCT

2.1 Optical circuit and force analysis of FOCT

Figure 1 shows the optical circuit structure of FOCT as the mainstream scheme [4]. The natural light from a super-luminescent diode (SLD), which has a center wavelength of 1,310 nm, is converted into a linearly polarized light along the x-axis (slow axis) of the panda PMF after passing through a fiber coupler and a polarizer. The linearly polarized light is split into two orthogonal linearly polarized lights after entering the next PMF through the 45° fusion point one. The two orthogonal linearly polarized beams are changed into left-handed and right-handed fundamental mode lights after passing through the 45° fusion point two and $\lambda/4$ wave plate. The lights enter a fiber sensing coil and are reflected back to the $\lambda/4$ wave plate by the reflector at the end of

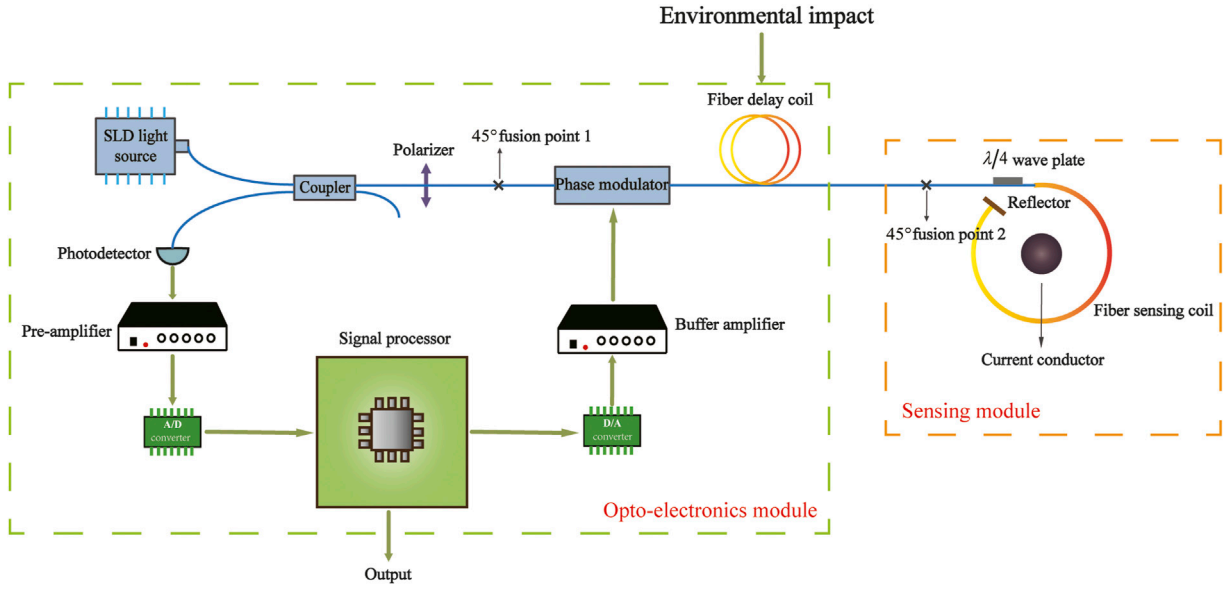

FIGURE 1
The schematic diagram of the in-line Sagnac FOCT structure.

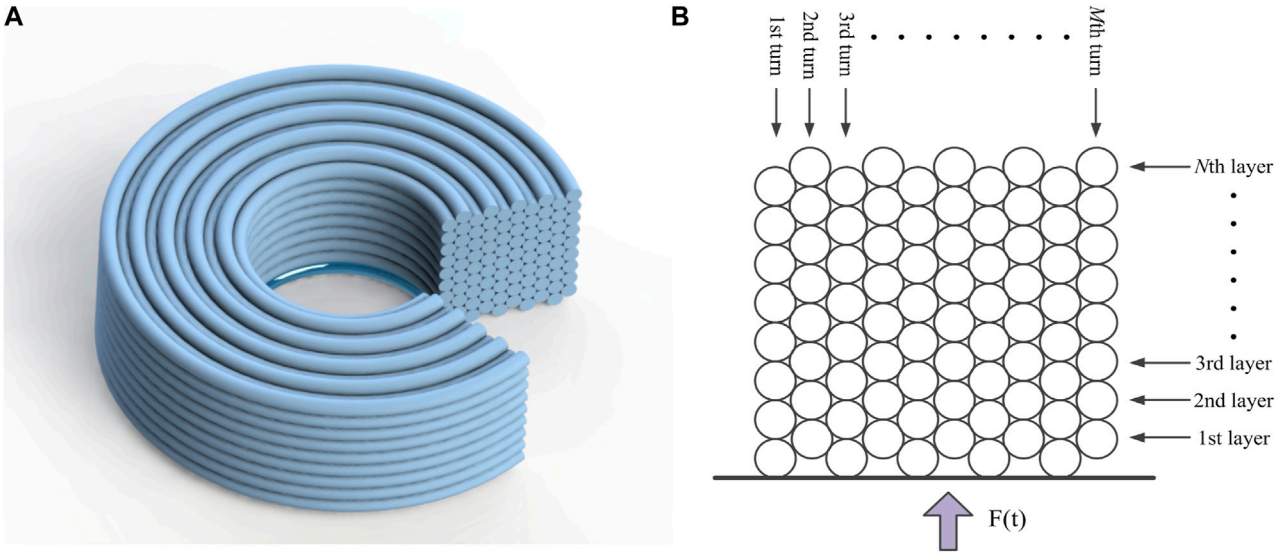

FIGURE 2
The structural diagram of PMF delay coil. **(A)** The three-dimensional structure of the PMF delay coil. **(B)** The side view structural diagram of the PMF delay coil.

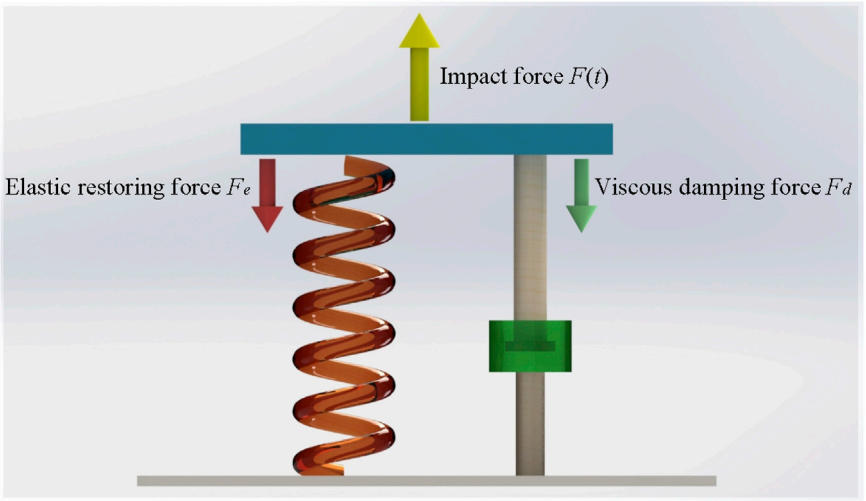

FIGURE 3
The equivalent model of the PMF delay coil system.

the optical fiber to change back to the linearly polarized light at the same time. The information of the measured current carried in the optical signal is finally interfered with by two linearly polarized light beams at the polarization, and the optical signal is converted into an electrical signal by a photoreceptor. Finally, the information of the measured current is outputted as a digital signal by a signal processing system.

When a FOCT is affected by external impacts, only the photoelectric devices related to optical fiber are influenced. Since the lengths of the fiber coupler, phase modulator, and $\lambda/4$ wave plate are very short compared to the length of the PMF delay coil and fiber sensing coil, the effect of impacts on these devices can be ignored. With respect to the fiber sensing coil, based on the analysis of the above system, the relative magnitude that the impacts brought to the left-handed and right-handed fundamental mode light and their respective polarization directions are small and can also be ignored. Therefore, the PMF delay coil is affected mostly by the impacts in FOCT. The above theoretical analysis has also been verified by the experimental results of Ref. [11]. Therefore, only specific force analysis will be conducted on the PMF delay coil.

When a ship is sailing in the sea, the impact on the ship's integrated power system generally comes from sudden changes in

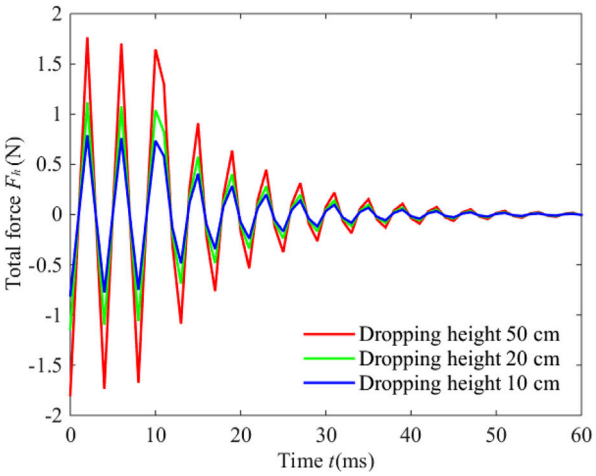

FIGURE 4
The curves of the variation of total force F_h with the time increase.

TABLE 1 Simulation parameters.

Parameters	Value
Impact time τ	10 m
Turns M	8
Layers N	10
The mass of PMF delay coil m_{coil}	7×10^{-11} kg (for 200 m length of the fiber)
Viscosity coefficient γ	0.2
Center optical wavelength of light source λ	1,310 nm
Original beat length of PMF L_{B0}	5.43 mm
Light speed c	3×10^8 m/s
Average refractive index n_0	1.45
Longitudinal elastic optical coefficient B_1	6.9×10^{-13} m^2/N
Transverse elastic optical coefficient B_2	41.9×10^{-13} m^2/N
Diameter of fiber D	250 μm
Turns of fiber sensing coil N_{sc}	10
Verdet constant of the fiber V	1.1×10^{-6} rad/A
Measured current I	640 A
Gravitational acceleration g	10 m/s^2
Damping coefficient η	0.01
Elasticity modulus of the fiber E	7×10^{10} Pa

the underwater environment, such as an explosion. Impact experiments usually use waveforms such as rectangular, semi-sinusoidal, and back-peak serrated to simulate different impacts. According to Refs. [12,13], the impulse signal can be equivalent to an ideal semi-sinusoidal pulse, and the change of its force over time can be expressed as

$$F_0(t) = \begin{cases} F_0 \sin\left(\frac{\pi}{\tau} t\right), & 0 \le t \le \tau \\ 0, & t > \tau \end{cases} \quad (1)$$

where τ represents the duration of impact received by the fiber delay coil of the polarization-maintaining fiber, and F_0 represents the amplitude of the function $F_0(t)$. t represents the time. The winding structure diagram of the PMF delay coil is shown in Figure 2.

Figure 2A shows the three-dimensional structure of the PMF delay coil [14]. Figure 2B shows the side structure of the delay coil. All fibers are closely connected using an ultraviolet-curing adhesive. It is defined that each horizontal line represents a layer wound of the optical fiber, and each vertical line represents a turning wound of the optical fiber. Assuming that the total number of the turning wound is M, and the number of layers is N, an optical fiber at any position is defined to be in the nth (n = 1, 2. . . .N) layer and mth (m = 1, 2. . . , M) turning. As can be seen from Figure 2B, there are dense arrangements between any two optical fibers. Considering that the actual conditions can only be suitable for simulated impulse experiments, the impact force applied on the PMF delay coils is in the vertical direction, and it is considered that the force between each turning wind of the fiber in the same layer is uniform. Under the above premise, we simplify the fixed model and consider that a small damped oscillation system is formed between each layer of fiber when the whole PMF delay coil is impacted. Subsequently, we establish the corresponding under-damping oscillation model with a single degree of freedom. To analyze the specific motion and force of the PMF delay coil, we need to carry out a two-step analysis. First, we need to consider the PMF delay coil as a whole system and analyze its motion and force. Then, based on the above conditions, we separately analyze the motion and force of each layer of the PMF delay coil. The motion and force of the whole PMF delay coil system are shown in Figure 3.

Here, the blue part represents the PMF delay coil whole system. The movement of the whole system can be considered equivalent to a simple harmonic vibration of a spring with gradual attenuation amplitude in the vertical direction, and the corresponding equation of motion is

$$m_{coil} \frac{d^2x}{dt^2} = F_0(t) - F_e - F_d \quad (2)$$

where m_{coil} represents PMF delay coil mass, $F_0(t)$ represents the external impact force, and F_e represents the elastic restoring force, which is equal to kx. k and x represent the stiffness coefficient and displacement in the vertical direction of the equivalent spring, respectively. F_d represents the viscous damping force, which is equal to $\gamma dx/dt$. γ and dx/dt represent the viscosity coefficient and velocity of spring, respectively. According to Eq. 2, the displacement of the spring x_1 during the process of impact ($t < \tau$) can be expressed as

$$\begin{aligned} x_1 &= be^{-\delta t} \sin\left(\sqrt{\omega_0^2 - \delta^2} \cdot t + \varepsilon\right) + b \sin(\omega t - \varepsilon) \\ b &= a_0 \Big/ \sqrt{\left(\omega_0^2 - \omega^2\right)^2 + 4\delta^2\omega^2} \\ \varepsilon &= \arctan\left[2\delta\omega / \left(\omega_0^2 - \omega^2\right)\right] \\ a_0 &= F_0 / m_{coil} = 2\sqrt{2gh_d}/\tau \end{aligned} \quad (3)$$

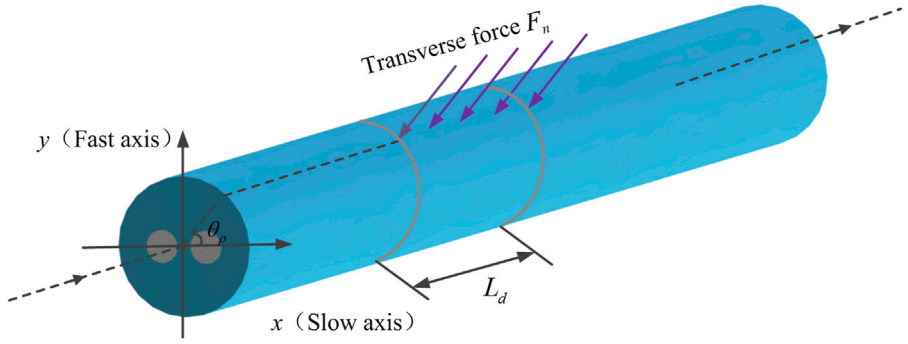

FIGURE 5
The diagram for the force analysis of PMF delay coil.

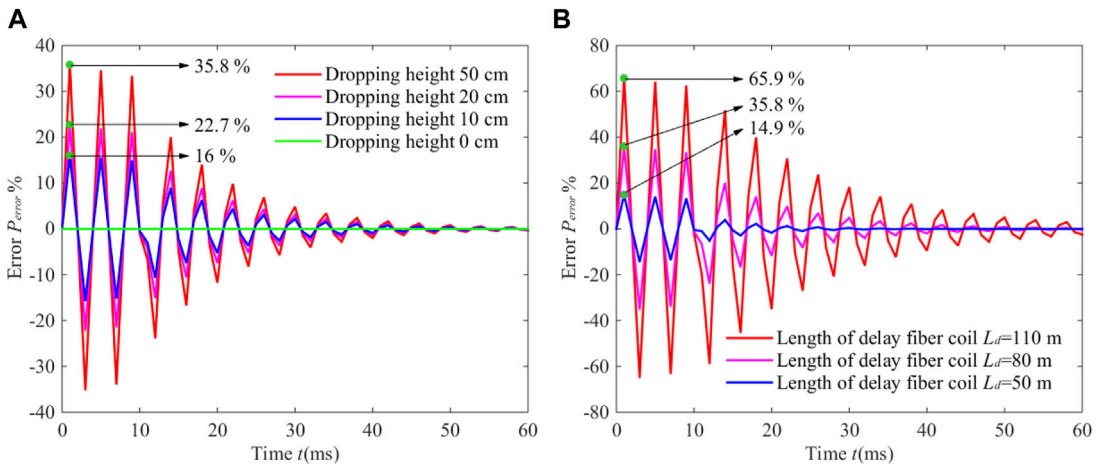

FIGURE 6
FOCT current measurement error caused by impacts under a PMF delay coil. **(A)** The variation of FOCT current measurement error with different free-fall heights when the length of the fiber delay coil is 80 m. **(B)** The variation of FOCT current measurement error with different lengths of fiber delay coil when the free-fall height is 50 cm.

where ω_0 represents the natural angular frequency of the whole system with the value of $\sqrt{k/m_{coil}}$, δ represents the damping coefficient of the whole system with the value of $\gamma/2m_{coil}$, ω represents the impact frequency with the value of π/τ, g represents gravitational acceleration, and h_d represents the falling height. When the impact is over ($t > \tau$), the displacement of spring x_2 can be calculated as

$$\begin{aligned} x_2 &= Ae^{-\delta t}\sin\left(\sqrt{\omega_0^2-\delta^2}\cdot t+\theta\right)\\ A &= \sqrt{x_0^2+(v_0+\delta x_0)^2/(\omega_0^2-\delta^2)}\\ \theta &= \arctan\left[\left(x_0\sqrt{\omega_0^2-\delta^2}\right)/(v_0+\delta x_0)\right] \end{aligned} \tag{4}$$

where x_0 and v_0 represent the displacement and velocity, respectively, of the equivalent spring when $t = \tau$. For each layer of the PMF delay coil, the whole motion is the same as the process described in Figure 3. According to Ref. [12], for the nth line fiber, the stiffness coefficient of the equivalent spring can be calculated as $k = E\Delta S/L$, and the damping coefficient of the fiber is η. E represents the elasticity modulus of the fiber. L represents the distance between the bottom of the fiber coil and each layer of the fiber with the value of $(2n\text{-}1)D/2$. ΔS represents the basal area of the fiber coil with the value of $(\sqrt{3}(M\text{-}1)L_dD)/(2NM)$. L_d represents the length of the PMF delay coil, and D represents the diameter of the fiber. Therefore, the stiffness coefficient k can be calculated as

$$k = \frac{\frac{\sqrt{3}}{2}(M-1)\frac{EL_dD}{N\times M}}{\frac{2n-1}{2}D} \tag{5}$$

In the actual process, when the whole system vibrates due to force, each line of the fiber and its coil bottom move simultaneously, and the corresponding dynamic equation of each line of fiber can be expressed as

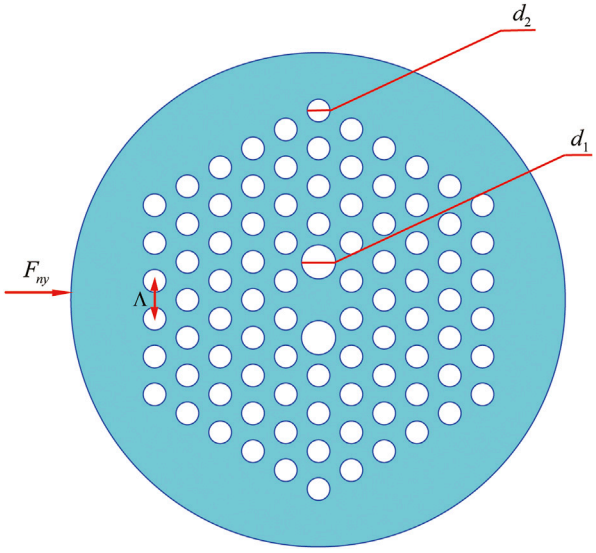

FIGURE 7
The cross-sectional structure diagram of the polarization maintaining PCF.

$$\begin{cases} \frac{m_{coil}}{N}\frac{d^2x}{dt^2} + \eta\left(\frac{dx}{dt} + \frac{dx_1}{dt}\right) + k(x + x_1) = 0, & 0 < t \le \tau \\ \frac{m_{coil}}{N}\frac{d^2x}{dt^2} + \eta\left(\frac{dx}{dt} + \frac{dx_2}{dt}\right) + k(x + x_2) = 0, & t > \tau \end{cases} \tag{6}$$

Here, the first differential equation of motion corresponds to the stage of continuous impact ($t < \tau$), and the second differential equation of motion corresponds to the stage of no impact ($t < \tau$). Finally, the solutions of Eq. 6 are

$$\begin{cases} x = e^{-\alpha_0 t}[C_1\cos(\beta t) - C_2\sin(\beta t)] - e^{-\alpha_0 t}\cos(\beta t)H + e^{-\alpha_0 t}\sin(\beta t)I, 0 < t \le \tau \\ x = e^{-\alpha_0 t}[C_3\cos(\beta t) - C_4\sin(\beta t)] - e^{-\alpha_0 t}\cos(\beta t)HH + e^{-\alpha_0 t}\sin(\beta t)II, t > \tau \end{cases} \tag{7}$$

According to Eq. 7, we can solve the impact force F_n of the nth layer PMF delay coil at two stages of $0 < t \le \tau$ (F_{1n}) and $t > \tau$ (F_{2n}). The total impact force F_h can be written as

$$F_h = \begin{cases} \sum_{i=1}^{n} F_{1n}, & 0 \le t \le \tau \\ \sum_{i=1}^{n} F_{2n}, & t > \tau \end{cases} \tag{8}$$

The specific values and names of all the symbols in Eqs 7, 8 are shown in the Supplementary Material S1. The relationship between F_h and t is shown in Figure 4. The simulation parameters can be found in Table 1 [13].

As shown in Figure 4, the change curve of force with time shows a sinusoidal trend of decay. During the first stage of $t \le 10$ ms, the external impact force plays a leading role, causing a small degree of attenuation of the total impact force. During the second stage of $t >$ 10 ms, there is no external impact force acting on the fiber delay coil. The damping of the ultraviolet curing adhesive plays a leading role, causing a gradual decrease in the amplitude of the total force. The higher the dropping height is, the smaller the total force will be. The results in Figure 4 prove that the total force variation trend over time is consistent with the motion process analyzed above.

2.2 Phase delay error of FOCT caused by impact

To simplify the force analysis mechanism and process of the optical fiber, the force analysis of the nth layer of the PMF delay coil is carried out in this study, and the force analysis diagram of the layer is shown in Figure 5 [15].

Figure 5 represents the diagram for the force analysis of the PMF delay coil. There is a transverse force F_n in the fiber; from the direction of the force, the x-axis is deviated by an angle θ_ρ. n_x and n_y are the refractive indices of the x and y-axes of the PMF delay coil, respectively. Δn is the linear birefringence of the PMF delay coil with a value of n_x-n_y. Considering the external force of the PMF delay coil, the refractive index of the axis of the PMF delay coil can be calculated according to Eq. 4 in Ref. [16].

$$\begin{cases} n_x = n_{x0} + B_1\sigma_x + B_2\sigma_y \\ n_y = n_{y0} + B_1\sigma_y + B_2\sigma_x \end{cases} \tag{9}$$

where n_{x0} and n_{y0} represent the original refractive index without the external force of the x and y-axes, respectively. σ_x and σ_y represent the transverse stress along the x and y-axes, respectively. B_1 and B_2 represent the longitudinal and transverse elastic optical coefficients, respectively. The specific equations for stress are

$$\begin{cases} \sigma_x = \frac{2F_{ny}}{\pi L_d D} \\ \sigma_y = -\frac{6F_{ny}}{\pi L_d D} \end{cases} \tag{10}$$

where F_{ny} denotes the component of the external force F_n along the y-axis with a value of $F_n\sin\theta_\rho$. According to Eqs 9, 10, the relationship between Δn and F_n is

$$\Delta n = \left(n_{x0} - n_{y0}\right) + \frac{4F_n\sin\theta_\rho}{\pi L_d D}(B_1 - B_2) \tag{11}$$

In practice, the angle between the direction of the external force and that of the x-axis is a residual value. Hence, we need to consider the greatest effect of the impact on the fiber. So, we consider a maximum value of 90° for the residual value. The above analysis focused on the change of the birefringence of any layer of the fiber under impact, and the extra phase error is marked as $\Delta\phi_{sn}$ and obtained by summing up the phase error of each layer. According to Eq. 4 in Ref. [10], the specific equation for the extra phase error is

$$\Delta\phi_s = \sum_{n=1}^{n}\Delta\phi_{sn} = \sum_{n=1}^{n}\frac{2\pi L_d}{L_B^2}\frac{\partial L_B}{\partial F_n}\frac{\partial F_n}{\partial t}\tau_{sn} \tag{12}$$

where L_B represents the beat length of the PMF delay coil and is equal to $\lambda/\Delta n$. λ denotes the center optical wavelength of the light source, and τ_{sn} represents the light transmission time of a single-layer PMF delay coil and is equal to $n_0 L_d/c$. c and n_0 represent the light speed and average refractive index of fiber, respectively. According to Eqs 8, 11, 12, the final current measurement error can be simplified as

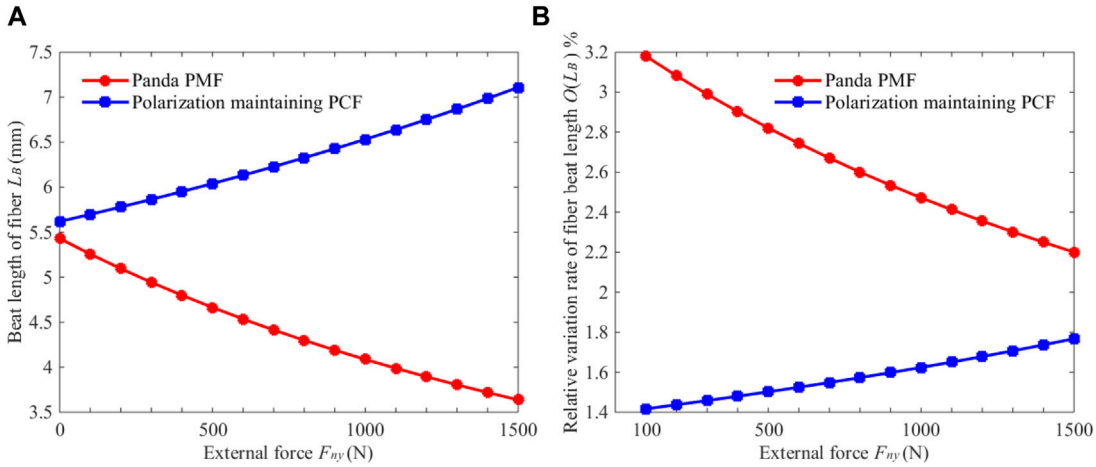

FIGURE 8
(A) The beat length variation with the change of force of the two kinds of fiber. **(B)** The beat length relative variation rate with the change of force of two kinds of fiber.

$$P_{error} = \frac{\Delta\phi_s}{4N_{sc}VI} = \frac{2\lambda n_0 L_d (B_1 - B_2)\sin\theta_\rho}{cDL_{B0}^2 \Delta n^2 N_{sc} VI} \cdot \sum_{n=1}^{n} \frac{\partial F_n}{\partial t} \quad (13)$$

where N_{sc} represents the number of turns of the fiber sensing coil, V represents the Verdet constant of the fiber sensing coil, and I denotes the measured current. From Eq. 13, the simulation results of the current measurement error of FOCT caused by impacts are shown in Figure 6. The simulation parameters can be found in Table 1.

As can be seen from Figure 6, the error of the fiber delay coil reaches the maximum value when the time duration of impacts is less than 10 ms, and the error at each peak value almost does not attenuate and is close to the maximum error value. When the time duration lasts for more than 10 ms, the error decreases over time and becomes even smaller when the time duration reaches 60 m. As can be seen from Figure 6A, the peak error decreases with the decrease in the free-fall height of the FOCT. The peak errors of the FOCT in free falling at 50, 20, and 10 cm are 35.8, 22.7, and 16%, respectively. As can be seen from Figure 6B, with the shortening of the length of the fiber delay coil, the peak error also decreases gradually. The peak errors corresponding to the lengths of 110, 80, and 50 m are 65.9, 35.8% and 14.9%, respectively. The above results proved that the phase error of the FOCT will be affected by different impact forces or changes in the fiber length of the fiber delay coil during the impacts.

3 Theoretical analysis of the polarization maintaining PCF

It can be seen from Eq. 13 that the phase error of the FOCT induced by impacts is mainly affected by its length, the beat length of the PMF delay coil, the beat length variation rate with the force, and the force variation rate with time. The change of force with time is determined by the external environment. In a panda PMF, the beat length is generally fixed. The length of optical fiber is mainly affected by the modulation speed of the FOCT circuit, so the choice of length reduction for phase error minimization is limited. Therefore, to greatly reduce the phase error, the way of reducing the sensitivity to forces of the beat length should be followed. The beat length of the fiber is related to the linear birefringence, and the linear birefringence of the fiber can be considered as the linear birefringence of the fiber core. The fundamental reason why the linear birefringence of the fiber changes with the force is the elastic effect. Therefore, from the perspective of weakening the elastic effect of the fiber core, polarization maintaining PCF can fundamentally solve the problem of the high sensitivity of linear birefringence of the fiber to force [17]. Reference [18] also pointed out that the air hole covering of the PCF can effectively reduce the influence of the elastic optical effect of the fiber core.

3.1 Force analysis of polarization maintaining PCF under impacts

The structure of the polarization maintaining the PCF of this research is shown in Figure 7. The cross-sectional structure of the polarization-maintaining PCF shown in Figure 7 contains five layers, and the air holes in each layer are arranged in a hexagonal pattern. Among the six air holes in the innermost layer, the diameters d_1 of two holes are larger than the diameters d_2 of the other air holes, and the distance between every two adjacent holes is Λ (lattice constant). Although the polarization maintaining PCF is not only limited to this structure, the panda PMF is adopted in the fiber tails of all the optical devices in the FOCT system. Therefore, the optical fiber with the structure shown in Figure 7 as the fiber delay coil of FOCT can make the mode fields between fibers more similar, allowing easier axis fusion and ensuring relatively small fusion loss. As for the force of the fiber, although the direction of force cannot be determined, it can be clearly seen from Eq. 11 that when the force direction of the fiber coincides with the y-axis (fast axis) of the fiber, the linear birefringence caused by elastic optical effect changes the most. Meanwhile, the polarization maintaining PCF of this structure is similar to the ordinary panda PMF structure. Although Eq. 11 cannot be completely used for quantitative analysis, its properties are similar to those of the panda PMF, so the

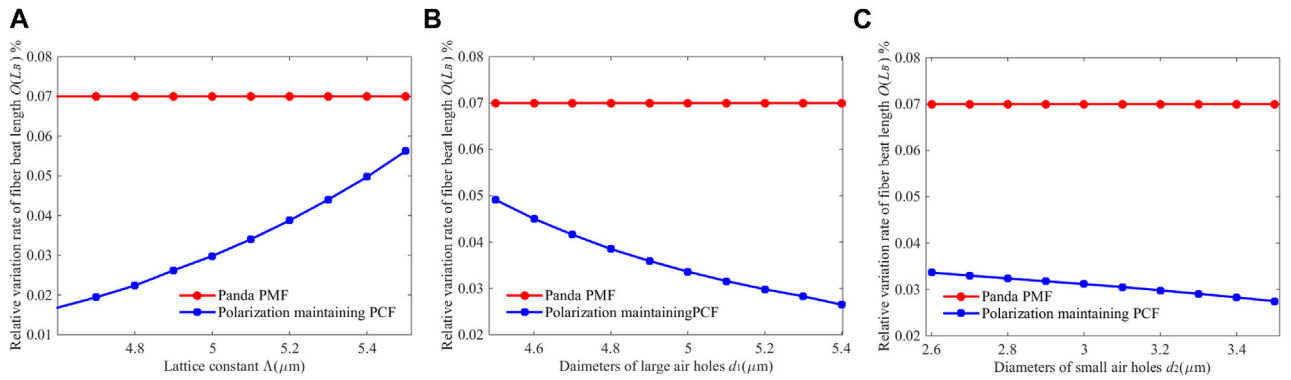

FIGURE 9
(A) The variation of relative change rate O (L_B) of beat length of fiber with the change of lattice constant Λ, d_1 = 5.2 μm and d_2 = 3.2 μm. **(B)** The variation of relative change rate O (L_B) of beat length of fiber with the change of large air holes d_1, Λ = 5 μm, and d_2 = 3.2 μm. **(C)** The variation of relative change rate O (L_B) of beat length of fiber with the change of small air holes d_2, d_1 = 5.2 μm and Λ = 5 μm.

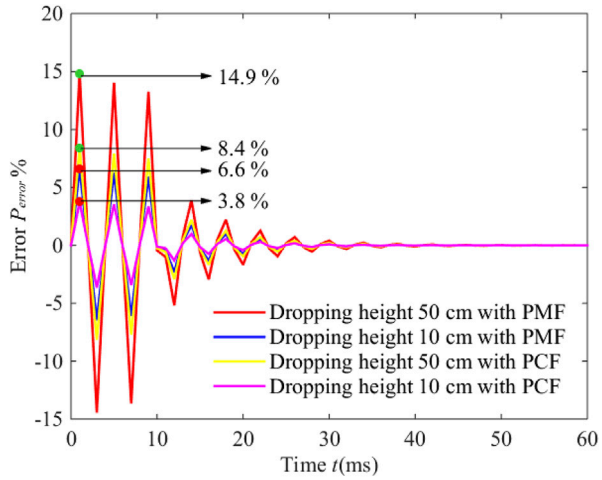

FIGURE 10
The current measurement error caused by FOCT after using polarization maintaining PCF with optimized parameters as the fiber delay coil.

same qualitative analysis method as the one in the case of the panda PMF can be used. In addition, since we believe that the optical fiber receives a uniform force in the vertical direction and the changes in the length and refractive index of the optical fiber in the vertical direction can be ignored, the force of the optical fiber can be simplified as two-dimensional. The force direction of the polarization maintaining PCF is marked in Figure 7.

Combined with a finite element method according to Eq. 11, we gradually increase the stress of the two kinds of optical fibers, and the relationship between the change of fiber beat length and the change of force can be obtained, respectively, as shown in Figure 8A. The red solid line represents the panda PMF, while the blue full line represents the polarization maintaining PCF. The parameters corresponding to the two kinds of optical fiber in the simulated experiment can be found in Table 1.

Although it can be seen from Figure 8A that the beat length of the two kinds of optical fibers changes with the increase of the force, it cannot be intuitively seen which optical fiber beat length is less sensitive to the external force. Therefore, we defined the relative change rate O (L_B) of an optical fiber (when the beat length changes with the force of the optical fiber) as

$$O(L_B) = \left| \frac{L_B(F_{ny2}) - L_B(F_{ny1})}{L_B(F_{ny1})} \right| \times 100\% \quad (14)$$

In Eq. 14, L_B (F_{ny1}) and L_B (F_{ny2}) represent the beat lengths of the optical fibers corresponding to the initial and changed force condition, respectively. According to the original data of the beat lengths of the optical fiber corresponding to the force conditions in Figure 8A, the calculation and processing are performed according to Eq. 14. It can be concluded that the relative change rates of beat lengths of the two kinds of PMFs vary with their forces, as shown in Figure 8B. It can also be clearly seen from Figure 8B that during the process of the force increasing from 0 to 1,500 N, the relative change rate of beat length of panda PMF is always greater than 2.2%, while that of the polarization maintaining PCF is always less than 1.8%. Therefore, it can be proved from the results of the simulated experiment that, under appropriate structural parameters, the polarization-maintaining PCF has less sensitivity compared to the panda PMF to the beat length force, and the results are also consistent with those of Ref. [17]. Therefore, according to Eqs 12, 14, under the same force, compared with the panda PMF, the polarization-maintaining PCF has lower beat length change rates. As the fiber delay coil of FOCT, the polarization-maintaining PCF can reduce the current measurement error caused by impacts.

3.2 Optimization of structural parameters of a polarization maintaining PCF

To increase the impact resistance ability of the polarization maintaining PCF as a delay coil of FOCT, we need to analyze and

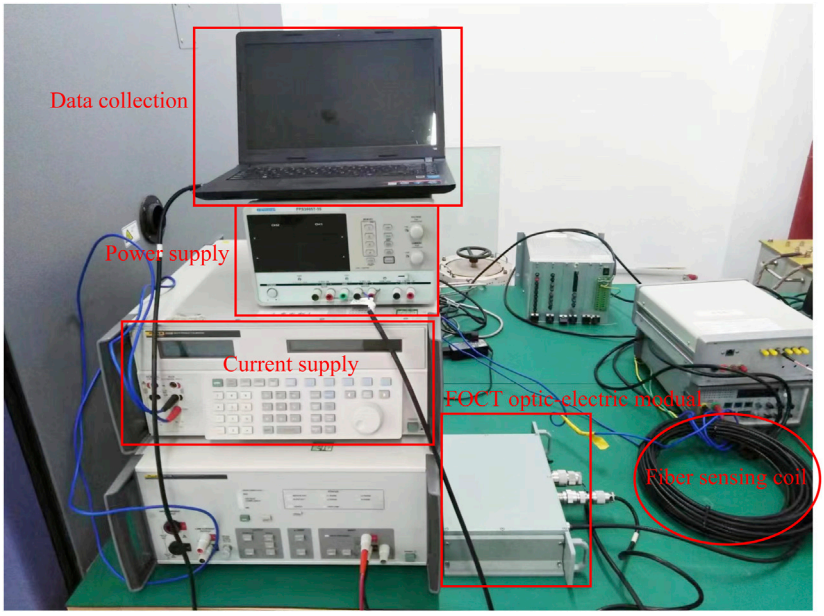

FIGURE 11
The process of the simulated impact experiment.

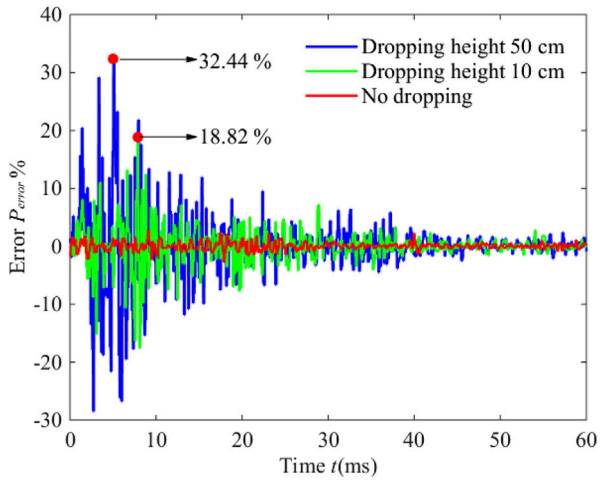

FIGURE 12
The actual current measurement error of the FOCT under different free-fall heights.

optimize the structural parameters of the air holes of the optical fiber. In the polarization maintaining PCF, the main structural parameters are the diameters of the two larger air holes (d_1), the diameters of smaller outer air holes (d_2), and the lattice constant (Λ) of the optical fiber. The influence of the changes of each of these three parameters on the relative change rate of the beat length is studied under the same force with the other two parameters fixed. The simulated results are shown in Figure 9, where the red solid line represents the panda PMF, and the blue solid line represents the polarization maintaining PCF.

It can be clearly seen from Figure 9A that for polarization maintaining PCFs, the relative change rate of the corresponding fiber beat length increases from 0.02% to 0.06% with the increase of lattice constant. As can be observed from Figures 9B, C, the increase of diameters d_1 and d_2, respectively, decreases the relative change rate of the optical fiber beat length. In particular, the change of diameters of the larger air holes has a greater impact on the relative change rate of optical fiber beat length compared to the change of diameter of the smaller air holes. Notably, the relative change rate of optical fiber beat length decreases from 0.05% to 0.027% and from 0.034% to 0.028% for the change of the larger and smaller holes' diameters, respectively. The reason for the above results is that the decrease of lattice constant or the increase of the diameters of the air holes increases the filling ratio of air in the fiber. In fact, the function of air holes can be equal to that of the protective layer of the optical fiber core, which can reduce the interference of external force when the light is transmitted in the fiber core. The increase of the air-filling ratio further reduces such interference, weakens the change of refractive index caused by the elastic optical effect, and reduces the force sensitivity of the optical fiber beat length. If the changes in the diameters of the air holes remain the same, compared with the smaller air holes, the increase in the diameter of larger air holes can significantly reduce the relative change rate of the optical fiber beat length. The reason for this significant reduction is that the increase in the diameter of the larger air holes can significantly change the optical fiber beat length. So, in conclusion, the range of the relative change rate of the optical fiber beat length of large air holes is more obvious.

To further reduce the influence that impacts bring to the beat length of the polarizing maintaining PCF delay coil and taking the

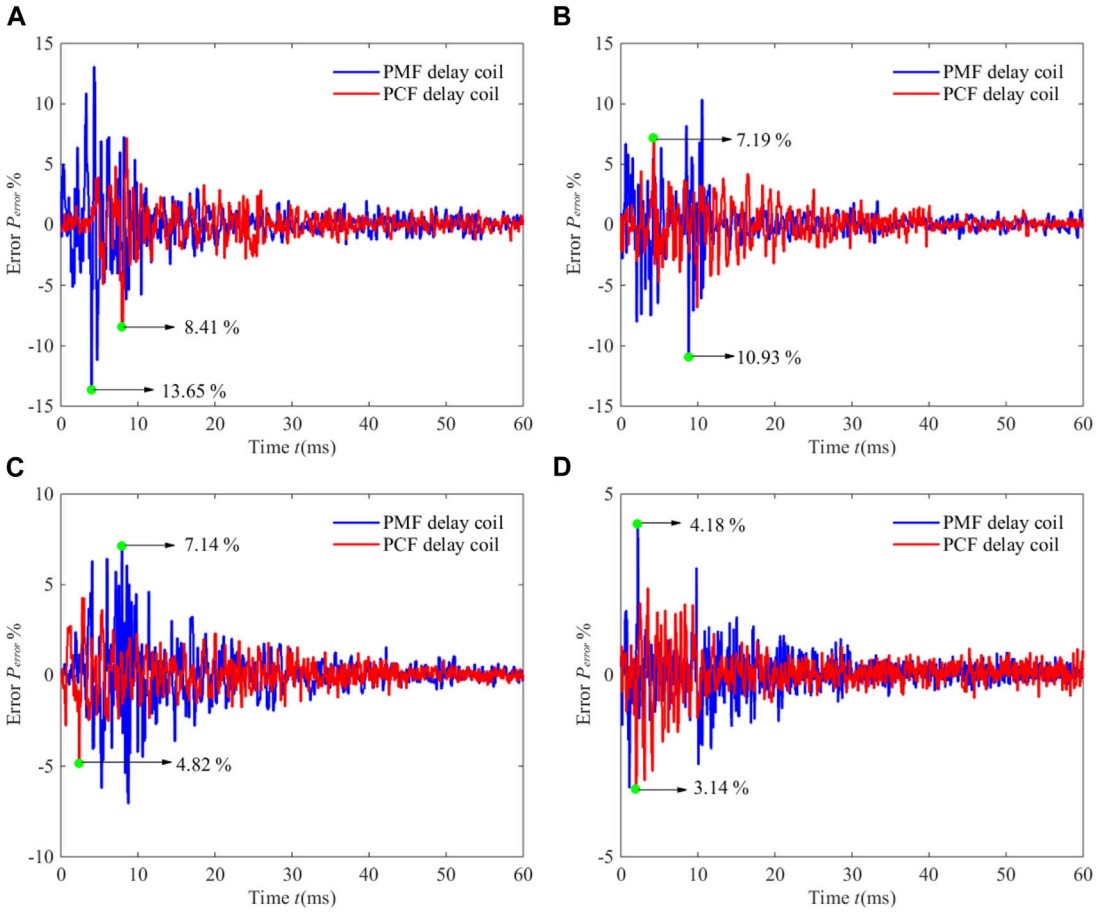

FIGURE 13
The comparison of current measurement errors of two kinds of fiber delay coils with different free-fall heights. **(A)** 50 cm free falling height. **(B)** 20 cm free falling height. **(C)** 10 cm free falling height. **(D)** 5 cm free falling height.

TABLE 2 The comparison of current measurement errors with two kinds of FOCT fiber delay coils.

Free falling height	Current measurement error with PMF the delay coil (%)	Current measurement error with the polarization maintaining PCF the delay coil (%)
50 cm (63 g)	13.65	8.14
20 cm (40 g)	10.93	7.19
10 cm (28 g)	7.14	4.82
5 cm (20 g)	4.18	3.14

mathematical rationality of the actual size of the optical fiber and the possibility of production into account, the structural parameters of the optical fiber are designed accordingly. The final values are lattice constant $\Lambda = 4.8$ μm, $d_1 = 5$ μm, and $d_2 = 3$ μm. According to Eq. 13, the decrease in the length of the fiber delay coil can also reduce the aftermath brought by impacts. However, considering the limitation brought by the modulation period of the FOCT signal processing unit, the length of the fiber delay coil is reduced to 50 m here. After the polarization maintaining PCF corresponding to the above structural parameters serves as the fiber delay coil of the FOCT, the additional phase delay error curve diagram can be obtained during impacts according to Eq. 13. The diagram is shown in Figure 10.

As can be seen in Figure 10, for a 50 m-long fiber delay coil, when the free falli height of the FOCT is 50 cm, the current measurement error of FOCT with the polarization maintaining PCF delay coil is reduced to 8.4%, compared to the 14.9% with the PMF delay coil. When the free fall height of the FOCT is 10 cm, the current measurement error of the FOCT with the PCF delay coil is reduced to 3.8% compared with the 6.6% error of FOCT with the PMF delay coil. The above results proved that the FOCT with the polarization maintaining PCF delay coil can reduce

the influence of extra phase error caused by impacts better in theory.

4 Comparison and analysis of experiment results

4.1 The verification of the current measurement error model

To verify the reasonableness of the impact-induced FOCT current measurement error model, PMF was adopted as the optical fiber delay coil of the FOCT, the length of which was set at 80 m. Other relevant parameters were consistent with the parameters in Table 1. The specific experimental process is shown in Figure 11.

In the experiment, we simulate the effect of free fall impact on the whole FOCT from free-fall under different heights of the photoelectric module of the FOCT. First, the height of the free-fall is measured to the left side of the FOCT photoelectric module and marked. Then, the FOCT photoelectric module is lifted to the height of the marked position. Finally, the FOCT photoelectric module is allowed to free fall and the impact is captured by the data acquisition software.

The free-fall height of the FOCT photoelectric module is set to 50 and 10 cm, respectively, and the actual current measurement error of the FOCT can be obtained, as shown in Figure 12.

As can be seen from Figure 12, when the height of the FOCT in free falling is 50 and 10 cm, the corresponding peak current measurement errors are 32.44% and 18.82%, and both errors reach the peak within 10 ms. After 10 ms, the errors corresponding to the two free-fall heights tend to decrease gradually, and the errors can be reduced to the range of noise current at about 60 ms. The results are roughly the same as those shown in Figure 6A in terms of trend and peak current errors, which can prove the rationality and accuracy of the impact-induced error model in this paper.

4.2 Comparison of current measurement errors of two kinds of optical fibers as the fiber delay coils results

To verify the error suppression effect under the impact of the polarization maintaining PCF as the FOCT fiber delay coil, we conducted a comparative experiment of polarization maintaining PCF and PMF as the FOCT fiber delay coils, respectively. The lengths of the two optical fiber delay coils are 50 m, and the free-fall heights of the FOCT photoelectric module are 50, 20, 10, and 5 cm, respectively. The corresponding current measurement errors are shown in Figure 13, and the specific values are shown in Table 2.

For the convenience of comparison, the current measurement error values marked in Figure 13 are all absolute values. As can be seen from Figure 13 and Table 2, compared with the FOCT corresponding to the PMF delay coil, the peak current measurement error in the FOCT using the polarization maintaining PCF delay coil reduced by about 35%, which proved that the method of using polarization maintaining PCF as the FOCT delay coil can reduce the current measurement error caused by impacts more effectively.

5 Conclusion

In this article, the forces on the polarization-maintaining fiber (PMF) delay coil of a fiber optic current transformer (FOCT) under environmental impact were investigated, and a current measurement error model based on the delay coil winding method was established. Also, the essential correlation of linear birefringence with phase error and current measurement error was derived. According to the proposed model, both the magnitude and force sensitivity of the beat length of fibers contribute to current measurement errors induced when FOCT is impacted. Apart from reasonably reducing the delay coil length, a polarization-maintaining photonic crystal fiber (PCF) is proposed as the delay coil of FOCT to reduce its phase error under impact conditions. Changes in linear birefringence of fibers under stress were also analyzed based on the structural parameters of different cross-sections of polarization maintaining PCF to optimize its structural parameters. This analysis thereby demonstrated by numerical simulation that the fluctuation of the linear birefringence of the polarization maintaining PCF under environmental impact is reduced by optimizing the structural parameters. In addition, the current measurement errors of FOCT with the two delay coils under environmental impact were investigated. The current measurement errors of FOCT based on the PMF delay coil in cases of different free fall heights obtained by measurements were compared with corresponding simulation results. The proposed current measurement error model is accurate for the FOCT under environmental impact. The current measurement results of FOCT with PMF and polarization maintaining PCF as the delay coil, respectively, in cases of different free-fall heights were compared. The comparison demonstrated that the FOCT with optimized polarization maintaining PCF as the fiber delay coil shows less current measurement error than the FOCT with PMF as the fiber delay coil. Specifically, the peak error of the current measurement of FOCT with the polarization maintaining PCF as the fiber delay coil was 35% less than that with the PMF as the fiber delay coil when the delay coil has a length of 50 m. Hence, the polarization maintaining PCF as the delay coil in FOCT provides an effective measure for the improvement of the environmental impact adaptability of the FOCT.

Data availability statement

The raw data supporting the conclusion of this article will be made available by the authors, without undue reservation.

Author contributions

All authors listed have made a substantial, direct, and intellectual contribution to the work and approved it for publication.

Funding

This work was supported by the National Natural Science Foundation of China (52271315, 51909048), the China Postdoctoral Science Foundation (2019T120260), the Heilongjiang Postdoctoral Science Foundation (LBH-TZ1015), and the Fundamental Research Funds for the Central Universities.

Conflict of interest

FY was employed by Shaanxi Dongfang Aviation Instrument Co., Ltd.

The remaining authors declare that the research was conducted in the absence of any commercial or financial relationships that could be construed as a potential conflict of interest.

Publisher's note

Supplementary material

The Supplementary Material for this article can be found online at: https://www.frontiersin.org/articles/10.3389/fphy.2023.1192965/full#supplementary-material

References

1. Chung Y, Liu WX, Schoder K, Cartes DA Integration of a bi-directional DC–DC converter model into a real-time system simulation of a shipboard medium voltage DC system. *Electr Power Syst Res* (2011) 81:1051–9. doi:10.1016/j.epsr.2010.12.010

2. Bohnert K, Gabus P, Nehring J, Brandle H Temperature and vibration insensitive fiber-optic current sensor. *J Lightwave Technol* (2002) 20(2):267–76. doi:10.1109/50.983241

3. Zhang F, Lit JWY Temperature and strain sensitivity measurements of high-birefringent polarization-maintaining fibers. *Appl Opt* (1993) 32(13):2213–8. doi:10.1364/ao.32.002213

4. Short SX, de Arruda JU, Tselikov AA, Blake JN Elimination of birefringence induced scale factor errors in the in-line Sagnac interferometer current sensor. *J Lightwave Technol* (1998) 16(10):1844–50. doi:10.1109/50.721071

5. Li YS, Zhang WW, Liu XY, Liu J Characteristic analysis and experiment of adaptive fiber optic current sensor technology. *Appl Sci* (2019) 9:333. doi:10.3390/app9020333

6. Qi YF, Wang MJ, Zhang FX, Zhang X, Cong BT, Liu YY Novel fiber optic current transformer with new phase modulation method. *Photonic Sensors* (2020) 10(3):275–82. doi:10.1007/s13320-020-0581-6

7. Roger AF, Moghaddam AA, Diaz ER, Vasquez JC, Guerrero JM J. Uceda. Dynamic assessment of COTS converters-based DC integrated power systems in electric ships. *IEEE Trans Ind Inform* (2018) 14(2):5518–29. doi:10.1109/TII.2018.2810323

8. Menis R, da Rin A, Vicenzutti A, Sulligoi G Dependable design of all electric ships integrated power system: Guidelines for system decomposition and analysis. In: IEEE conference: Electrical Systems for Aircraft, Railway and Ship Propulsion; 2-4 Nov 2016 (2012). p. 13193142.

9. Shen QY, Ramachandran B, Srivastava SK, Andrus M, Cartes DA Power and energy management in integrated power system. In: IEEE Electric Ship Technologies Symposium; 10-13 April 2011 (2011). p. 12008016.

10. Short SX, Tselikov AA, de Arruda JU, Blake JN Imperfect quarter-waveplate compensation in Sagnac interferometer-type current sensors. *J Lightwave Technol* (1998) 16(7):1212–9. doi:10.1109/50.701399

11. Short SX, Tantaswadi P, de Carvalho RT, Russell BD, Blake J An experimental study of acoustic vibration effects in optical fiber current sensors. *IEEE Trans Power Deliv* (1996) 11(4):44–5. doi:10.1109/mper.1996.4311007

12. Gao ZX, Zhang YG, Zhang Y Modeling for IFOG vibration error based on the strain distribution of quadrupolar fiber coil. *Sensors* (2016) 16:1131. doi:10.3390/s16071131

13. He XM, Wang GC, Gao W, Wang YG, Gao HZ The effect analysis of impact on a fiber optic current sensor. *Optik* (2021) 238:166724. doi:10.1016/j.ijleo.2021.166724

14. Wang ZC, Wang GC, Wang YY, Wang Z, Gao W Research on the birefringence distribution of the fiber coil with quadrupole symmetrical winding method. *IEEE Sensors J* (2022) 22(4):3219–27. doi:10.1109/JSEN.2021.3139626

15. Tsubokawa M, Higashi T, Negishi Y Mode couplings due to external forces distributed along a polarization-maintaining fiber: An evaluation. *Appl Opt* (1988) 27(1):166–73. doi:10.1364/ao.27.000166

16. Szpulak M, Martynkien T, Urbanczyk W Effects of hydrostatic pressure on phase and group modal birefringence in microstructured holey fibers. *Appl Opt* (2004) 43(24):4739–42. doi:10.1364/ao.43.004739

17. Li S, Li YB, Lv HW, Ji CT, Gao HZ, Sun Q Chiral dual-core photonic crystal fiber for an efficient circular polarization beam splitter. *Photonics* (2023) 10:45. doi:10.3390/photonics10010045

18. Zhu ZM, Brown TG Stress-induced birefringence in microstructured optical fibers. *Opt Lett* (2003) 28(23):2306–9. doi:10.1364/ol.28.002306